



Electrical properties of NiO-based composite ceramics modified by La_2MO_4 ($M = \text{Cu}$ or Ni) for NTC thermistors

Linling Huang¹, Hong Zhang¹, Senlin Leng², Mei Li¹,* and Zhicheng Li^{1,*}

¹School of Materials Science and Engineering, Central South University, Changsha 410083, China

²School of Material and Chemical Engineering, Tongren University, Tongren 554300, China

Received: 8 April 2023

Accepted: 20 April 2023

Published online:
12 May 2023

© The Author(s), under exclusive licence to Springer Science+Business Media, LLC, part of Springer Nature 2023

ABSTRACT

Negative temperature coefficient (NTC) thermistors are important for temperature sensors and actuators. In this work, La_2MO_4 ($M = \text{Cu}$ or Ni) modified NiO composite ceramics are prepared by conventional solid-state reaction method for NTC thermistors. All prepared composite ceramics have a main phase with a rock-salt structure of NiO and a second phase of La_2NiO_4 or La_2CuO_4 . The introduction of La_2CuO_4 or La_2NiO_4 significantly improved the sintering ability of ceramics and reduced the sintering temperature from 1380 °C of pure NiO ceramic to 1250 °C composite ceramics. For the existence of highly conductive La_2CuO_4 or La_2NiO_4 , the room temperature resistivity of ceramics can be effectively reduced, while the ceramics maintain NTC material constant higher than 4000 K. The electrical properties of ceramics were analyzed by combining with XRD, XPS, and complex impedance spectra. Several conduction modes such as band conduction, polaron hopping, percolation conduction, and grain-boundary transition of charge carriers are proposed for the electrical conductivity and NTC characteristics of NiO-based composite ceramics.

1 Introduction

Negative temperature coefficient (NTC) thermistors are characterized by resistivity decreasing with temperature increasing, especially, the resistivity decreases exponentially with temperature rising. Due to their high temperature sensitivity and fast response, NTC thermistors are widely used in the fields of electrical equipment, battery safety system, automobiles, medical apparatus, aerospace, etc., for suppressing impulse current, temperature

measurement, and temperature control, and so on. Room temperature resistivity (ρ_{25}) and material constant (B value) reflecting temperature sensitivity are two important parameters for an NTC thermistor. The B value can be determined by Eq. (1).

$$B = \frac{\ln \rho_1 - \ln \rho_2}{1/T_1 - 1/T_2} \quad (1)$$

where, ρ_1 and ρ_2 are resistivities at temperatures T_1 and T_2 , respectively.

Traditionally, ordinary-temperature NTC thermistors are usually composed of compounds with spinel-

Address correspondence to E-mail: zhchli@csu.edu.cn

or perovskite-type crystalline structures [1–5]. Where, spinel type materials are the most widely studied and applied ones for the NTC thermistors. In the same series of spinel type NTC materials, a small ρ_{25} is often accompanied by a small B value, a larger B value is accompanied by large ρ_{25} , and it is not easy to achieve coordinated control of B value and ρ_{25} . For practical applications, there is often a need for low resistance and high B value. The design of composite materials can effectively solve the coordination problem between B value and ρ_{25} [6, 7]. As reported by Zhou et al. [6], the composite ceramics made of spinel-structured $(\text{Ni,Mn})_3\text{O}_4$ and perovskite-structured $\text{La}(\text{Mn,Ni})\text{O}_3$, ρ_{25} could be reduced by one to two orders of magnitude depending on the amount of the low-resistivity perovskite phase $\text{La}(\text{Mn,Ni})\text{O}_3$, while the B values could still be large in a range of 3000–4000 K.

In the past years, the NTC thermistors based on simple oxides such as SnO_2 , CuO , ZnO , and NiO have been also reported [8–15], and have advantages of easy adjustment of ρ_{25} and B values over a wide range as well as the synergistic adjustability of both. NiO is a typical semiconductor oxide and shows potential applications in fields of magnetism, catalysis, gas sensors, dielectrics, thermoelectric, lithium-ion batteries, and supercapacitors [16–19]. The NTC thermistors based on simple oxides were always designed using the strategy of element doping and solid solution [8–12, 14, 15], but there is little work on the strategic approach of composite materials. La_2CuO_4 and La_2NiO_4 have high conductivities and were studied for the applications of mixed ionic electric conductors, photocatalysis, and magnetic properties [20–23].

In this work, NiO -based NTC composite ceramics modified by La_2CuO_4 and La_2NiO_4 were prepared, respectively. The electrical conductivity and NTC properties of NiO -based ceramics were studied. The results show that both La_2CuO_4 and La_2NiO_4 can enhance the sintering ability and reduce resistance of composite ceramics. All prepared ceramics show NTC material constants ($B_{25/85}$ value) above than 4000 K. The phase composition, microstructure, electrical properties, and conduction mechanisms of the prepared NiO -based NTC ceramics were investigated.

2 Experimental

NiO -based ceramics compound with different contents of La_2CuO_4 and La_2NiO_4 were prepared by traditional solid-state reaction processes. The selected raw materials are basic nickel carbonate ($\text{NiCO}_3 \cdot 2\text{Ni}(\text{OH})_2 \cdot 4\text{H}_2\text{O}$, $\geq 99.0\%$, Xilong Technology, China), lanthanum oxide (La_2O_3 , $\geq 98.0\%$, Xilong Technology, China), cupric oxide (CuO , $\geq 99.0\%$, Xilong Technology, China). According to the stoichiometric ratio of designed compounds, raw materials are calculated and weighed separately. The weighted raw materials were ground and mixed sufficiently in an agate mortar. The mixed powders were calcined at 900 °C and 5 h for NiO , 900 °C and 10 h for La_2NiO_4 , and 1000 °C 10 h for La_2CuO_4 .

In this work, ceramics of pure NiO , La_2CuO_4 , La_2NiO_4 , $\text{NiO-L}_2\text{CuO}_4$ composites, and $\text{NiO-L}_2\text{NiO}_4$ composites were, respectively, prepared by a traditional ceramic sintering technology. For NiO , La_2CuO_4 , and La_2NiO_4 ceramics, each of related calcined powders was granulated with appropriate amount of ethylene glycol as a binder, and then was pressed into green pellets with a diameter of 12 mm and a thickness of about 2.5 mm. For $\text{NiO-L}_2\text{CuO}_4$ (or $\text{NiO-L}_2\text{NiO}_4$) composite ceramics, the mass ratios of 0.5%, 1.5%, 3.0%, and 8.0% of prepared La_2CuO_4 or La_2NiO_4 powder were respectively selected, and the related samples are denoted as NiO-xLCO or NiO-yLNO , where, x and y are 0.5, 1.5, 3.0, and 8.0, respectively. According to the mass ratios of designed composites, NiO and La_2CuO_4 powders (or NiO and La_2NiO_4 powders) were weighed, mixed, and granulated, and then were pressed into green pellets with a diameter of 12 mm and a thickness of about 2.5 mm. Pure NiO ceramics were sintered at 1380 °C for 1 h, the composite ceramics were sintered at 1250 °C for 30 min. La_2CuO_4 and La_2NiO_4 ceramics were sintered at 1080 °C and 1250 °C for 1 h, respectively. For the measurement of electrical properties, the sintered ceramics were polished with sandpaper on both opposite sides and cleaned with ethanol, and then coated with silver paste on both sides followed by being heated to 600 °C for 5 min to form ohmic electrodes.

The phase composition of as sintered ceramics was characterized by X-ray diffractometer (XRD, Rigaku D/max 2500, Japan. Cu K_α radiation, $\lambda = 0.154056$ nm) with diffraction angles (2θ) between 20° and 80° at scanning speed of 8°/min,

and was analyzed using Jade 6.0 + pdf 2004 software. The ceramic microstructure was characterized by a field emission scanning electron microscopy (SEM, JMS-7900 F, Japan), and the analysis of element composition and distribution in ceramics was performed using X-ray energy dispersive spectroscopy (EDS) equipped with SEM. The valence state of cations in the studied ceramics was analyzed by X-ray photoelectron spectroscopy (XPS, K-alpha 1063, UK), high resolution spectra of elements were fitted and deconvoluted using an Avantage software.

The temperature dependence of resistance (R - T) of each ceramic was measured by R - T measurement system (ZWX-C, China), in temperature range from 25 to 250 °C. Resistivity (ρ) was calculated according to Ohm's law of $\rho = RA/h$, where A is electrode area, h is sample thickness, and R is sample resistance. To detect the electrical stability of the composite ceramics, aging treatment was performed at 150 °C for 500 h in air. The aging induced resistance change rates were defined by equation $\Delta R/R_0 = (R_1 - R_0)/R_0$, where R_0 and R_1 are resistances before and after aging, respectively, and were measured at room temperature (25 °C).

The alternating current (AC) complex impedance spectrum is obtained in the frequency range from 1 Hz to 1 MHz using an electrochemical test system (Gamry reference 600, USA). The resistances from grain effect and grain-boundary one of ceramics were obtained by analyzing each complex impedance spectrum (CIS) using a Gamry Echem analysis program combined with an appropriate equivalent circuit. Each CIS in the frequency range of 10^6 - 10^{10} Hz was further constructed by a Z-view software, according to the equivalent circuit.

3 Results and discussion

3.1 Phase and microstructure

Figure 1 shows XRD patterns of NiO, NiO- x LCO ($x = 1.5$ and 8.0), and NiO- y LNO ($y = 1.5$ and 8.0) as-sintered ceramics. The main diffraction peaks of all ceramics can be indexed as rock salt cubic structure, with space group of $Fm - 3m$ (225) (Ref. PDF No. 47-1049, lattice parameter $a = 0.4177$ nm). The XRD peaks at diffraction angles (2θ) of 37.3°, 43.2°, 62.9°, 75.5°, and 79.5° correspond to (111), (200), (220), (311), and (222) planes of the main crystalline phase NiO,

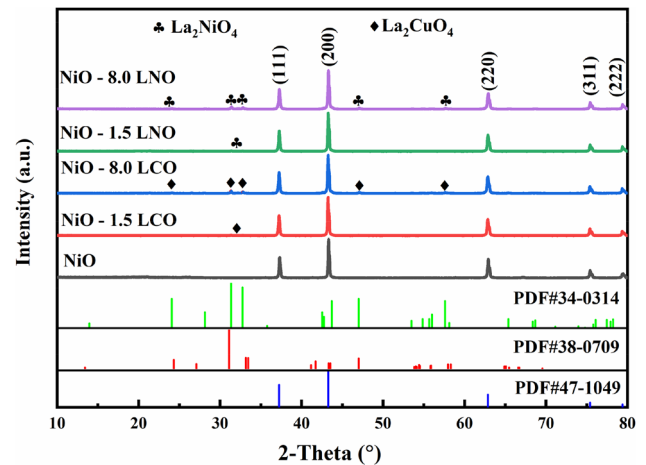
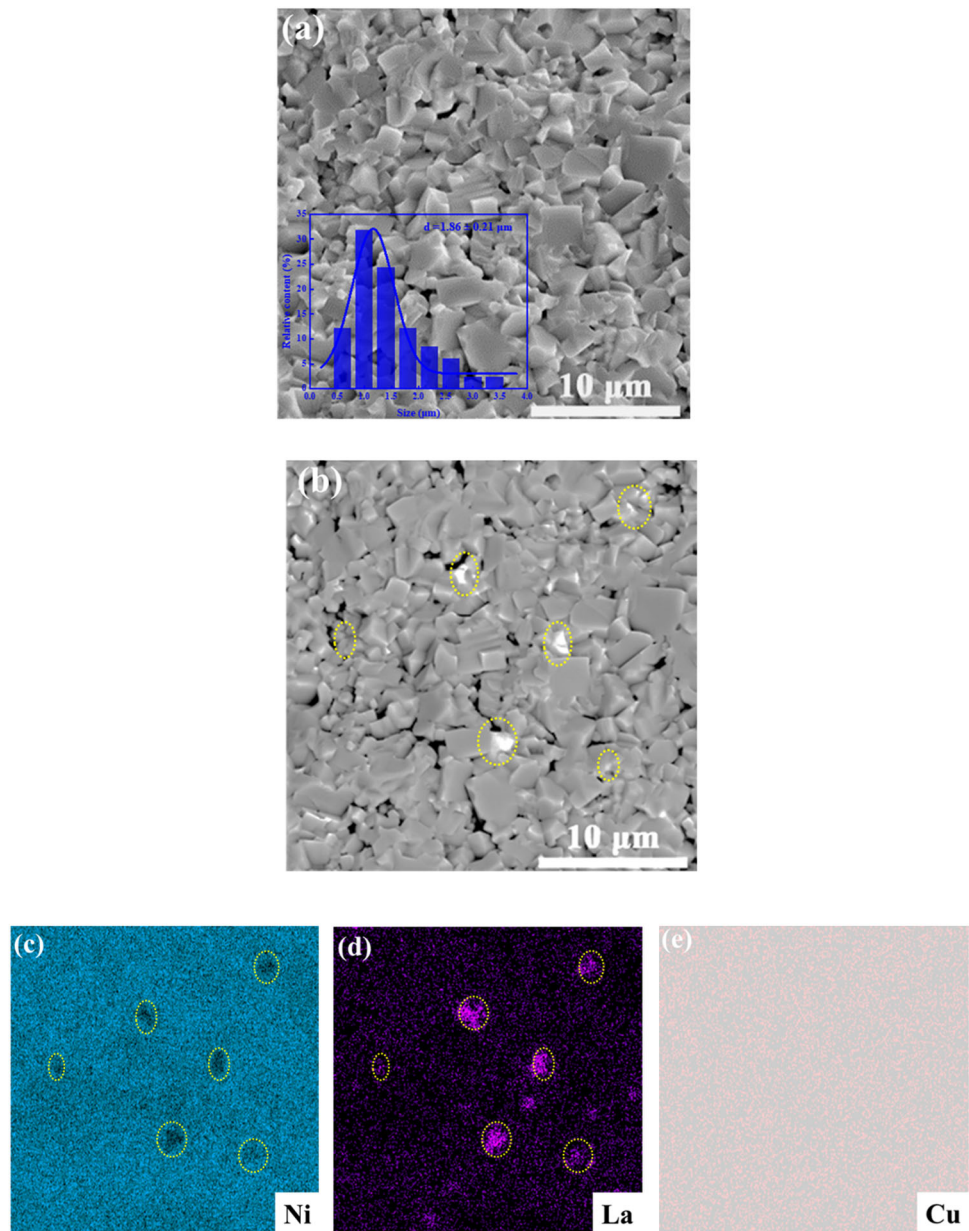


Fig. 1 Analysis of XRD patterns of as-sintered ceramics

respectively. In the XRD spectra of NiO- x LCO and NiO- y LNO composite ceramics, some diffraction peaks can be detected except for the ones of the primary phase NiO. The NiO-1.5LCO and NiO-1.5LNO ceramics have a diffraction peak at 2θ of 31.3°. While, the NiO-8.0LCO and NiO-8.0LNO ceramics have additional diffraction peaks 2θ at 32.8°, 47.0°, and 57.6°, which correspond to (103), (110), (200), (213) crystal planes of La_2CuO_4 or La_2NiO_4 (Ref. PDF No. 38-0709, and PDF No. 34-0314), respectively. The intensity of the additional diffraction peaks increases with the increase of La_2CuO_4 or La_2NiO_4 content. These indicate that La_2NiO_4 or La_2CuO_4 phase exists in the related ceramics, and the prepared NiO- x LCO and NiO- y LNO are composite ceramics. Refined by Jade 6.0 + pdf2004 program, lattice parameters (a) of NiO phase in the as-sintered pure NiO, NiO-1.5LCO, NiO-8.0LCO, NiO-1.5LNO, and NiO-8.0LNO are 0.4168, 0.4179, 0.4179, 0.4176, and 0.4178 nm, respectively. The lattice parameter (a) of pure NiO is less than that of referred PDF No. 47-1049 ($a = 0.4177$ nm). While, all the lattice parameters of NiO- x LCO and NiO- y LNO ceramics are larger than that in pure NiO ceramics. These indicate that the as-sintered NiO ceramics are consisted of defects such as vacancies. And partial La-ions might have substituted into NiO lattice in NiO- x LCO and NiO- y LNO ceramics, the radius of La-ion (0.117 nm) is larger than the one of Ni^{2+} ion (0.069 nm), and the substitution of La-ions enlarged the NiO lattice.

SEM images of calcined powders of pure NiO, La_2CuO_4 , and La_2NiO_4 are shown in Fig. S1 in the supplementary document. The powders show equiaxed-grain characteristics. Figure S2 provides an

Fig. 2 SEM investigation of NiO-1.5LCO ceramic, **a** secondary electronic image, **b** backscattered image, **c–e** EDS elemental distribution mapping of Ni, La, and Cu, respectively



SEM image of fracture surface in pure NiO ceramic. The as-sintered NiO ceramic shows grown-up equiaxed grains with an average grain size of about 1.2 μm , while the average grain size of as-calcined powder is about 0.3 μm .

Figure 2 shows SEM observation and EDS mapping of elements distribution of NiO-1.5LCO composite ceramic. Figure 2a is a secondary electronic image, and Fig. 2b is a backscattered SEM image taken from the same area as that in Fig. 2a. The average grain size is 1.86 μm . Figure 2c–e are elemental mappings of Ni, La, and O, respectively. From Fig. 2b, one can see some areas with bright contrast

as marked by circles could be La-rich regions according to the mapping in Fig. 2d. These La-rich regions are Ni-lack ones as shown in Fig. 2c. Combining the SEM observations with the XRD results in Fig. 1, one can obtain that the La-rich regions should be the La_2CuO_4 phase, although we could not get much information about the Cu-distribution from Fig. 2e for the low content and weak EDS signal. These indicate that the prepared NiO- x LCO ceramics are composed of NiO and La_2CuO_4 phases.

Similar to that of NiO-1.5LCO composite ceramic, NiO-1.5LNO composite ceramic was investigated by SEM. Figure 3a and b show the secondary electron

Fig. 3 SEM investigation of NiO–1.5LNO ceramic, **a** secondary electron image, **b** backscattered image, **c–e** EDS elemental mapping of Ni, La, and O, respectively

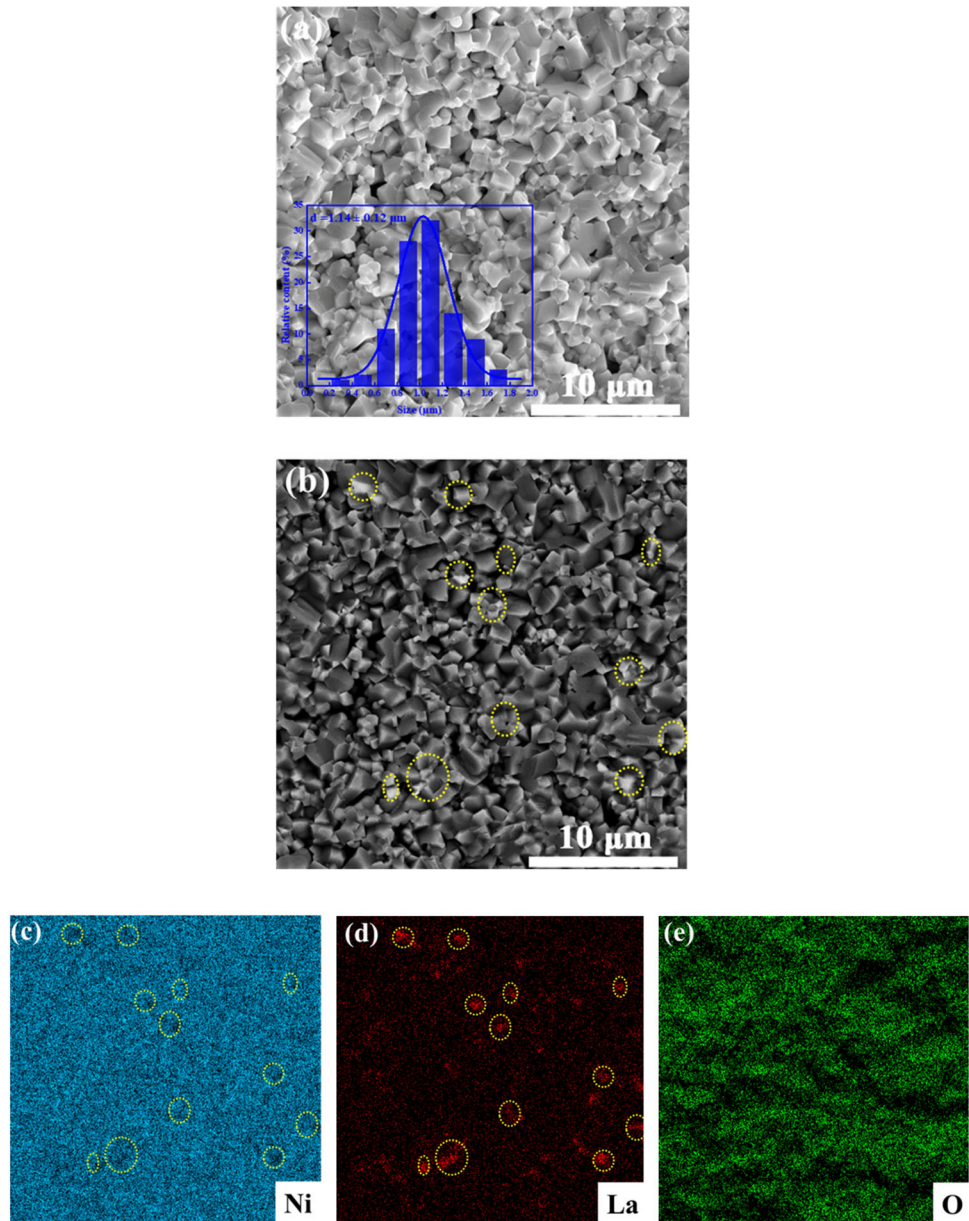


image and backscattered electron image of fracture surface in NiO–1.5LCO composite ceramic, and are recorded in the same area. In the backscattered electron image (see Fig. 3b), two kinds of contrasts (bright and gray ones) can be observed. Figure 3c, d and e show elemental mapping of Ni, La, and O, respectively. From Fig. 3b, one can deduce that the areas with bright contrast, as marked by circles, should be La-rich regions according to the mapping in Fig. 3d. The bright contrast regions in Fig. 3b are La-rich and Ni-lack ones (see in Fig. 3c and d). The EDS mapping of O element in Fig. 3e implies that O element is uniformly distributed in ceramics.

Combined with the XRD results in Fig. 1, the area with bright contrast should come from La_2NiO_4 , and the ones with gray contrast are NiO. These indicate that the prepared NiO- x LNO ceramics are composed of NiO and La_2NiO_4 phases.

By comparing the distribution characteristics of La_2CuO_4 and La_2NiO_4 in NiO–1.5LCO and NiO–1.5LNO composite ceramics as shown in Figs. 2 and 3, respectively, one can get that La_2NiO_4 has smaller grain size and is more evenly distributed in NiO–1.5LNO composite ceramics than La_2CuO_4 in NiO–1.5LCO composite ceramic. These should be related to the melting temperatures of La_2CuO_4 and

La₂NiO₄. The liquid phase occurs at about 1025 °C in La₂CuO₄, and liquid phase forms at about 1635 °C in La₂NiO₄ [24, 25]. So La₂CuO₄ liquid phase occurred during the sintering process of NiO-*x*LCO composites, and phase aggregating took place. These should also lead the particle size in NiO-1.5LCO composite ceramics to be larger than that in NiO-1.5LNO composite ceramics. SEM images of NiO-8.0LCO and NiO-8.0LNO are shown in Fig. S3.

3.2 XPS analysis of Ni-cation valence

XPS spectra of Ni element recorded for pure NiO ceramic, NiO-1.5LCO and NiO-1.5LNO composite ceramics were analyzed, respectively. The spectra of Ni 2p_{3/2} orbits are shown in Fig. 4. These XPS spectra were calibrated referring to the binding energy of 284.8 eV of C 1s. Each XPS spectrum consists of a main part (see the right part) and a subsidiary part (in the left part). The spectra were fitted and analyzed by Gauss-Lorentz curve, deconvoluted using an Avantage software. Each XPS spectrum can be fitted to be composed of six individual peaks. The peaks near 853 eV, 855 eV, and 860 eV should come from Ni²⁺ cations, while 856 eV, 857 eV, and 863 eV are from Ni³⁺ cations [26]. These indicate that Ni²⁺ and Ni³⁺ ions co-exist in the as-sintered ceramics. According to the areas of fitted peaks, the content ratios of Ni²⁺ and Ni³⁺ ions (denoted as [Ni²⁺]/[Ni³⁺]) in pure NiO ceramic, NiO-1.5LCO and NiO-1.5LNO composite ceramics are 2.69:1, 2.52:1 and 2.48:1, respectively.

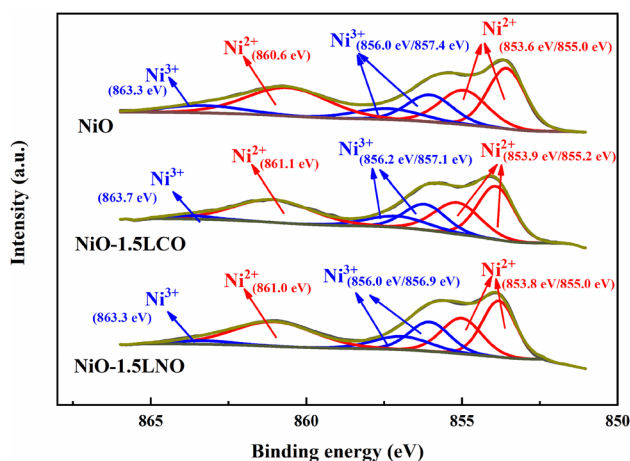


Fig. 4 Analysis of XPS for Ni element in composite ceramics of NiO-1.5LCO and NiO-1.5LNO

3.3 Electrical property

The resistance-temperature characteristics of prepared ceramics were investigated by measuring resistances at different temperatures. And resistivities were calculated using the measured resistances according to sample sizes. The electrical properties (temperature dependence of resistivity) of pure NiO, La₂CuO₄, and La₂NiO₄ ceramics are shown in Fig. S4. The NiO ceramic shows a typical NTC effect with ρ_{25} of 7807 Ω -cm and *B* value of 5563 K. Both La₂CuO₄ and La₂NiO₄ ceramics have quite low ρ_{25} of 5.2 Ω cm and 4.2 Ω cm, respectively. In the meanwhile, La₂MO₄ (*M* = Cu or Ni) modified NiO composite ceramics show high stability against temperature. As shown in Fig. S5, both NiO-1.5LCO NiO-1.5LNO composite ceramics have the resistance change rates lower than 0.25% after have being aged at 150 °C for 500 h.

Figure 5a and b show the resistance-temperature characteristics of NiO-*x*LCO (*x* = 0.5, 1.5, 3.0, 8.0) and NiO-*y*LNO (*y* = 0.5, 1.5, 3.0, 8.0) composite ceramics. The detailed ρ_{25} and *B*_{25/85} values of the composite ceramics are listed in Table 1. All ceramics have material constants *B*_{25/85} higher 4200 K. The introduction of both La₂CuO₄ and La₂NiO₄ decreased ceramic resistivity, compared to the resistivity of pure NiO ceramic. The ρ_{25} of NiO-*x*LCO composite ceramics decreased with increase of La₂CuO₄ content. While ρ_{25} of NiO-*y*LNO composite ceramics did not change significantly with the La₂NiO₄ content. As shown in Table 1, the room temperature resistivity of prepared ceramics can be reduced from 7807 Ω cm of pure NiO ceramic to 450 Ω cm of NiO-0.5LNO composite ceramic. As displayed in Fig. S4, La₂CuO₄ and La₂NiO₄ have very low resistivities, and can enhance the conductivity of NiO-based composite ceramics through the percolation effect. As analyzed in Figs. 2 and 3, La₂NiO₄ has a better dispersion distribution in the composite ceramics than La₂CuO₄. The more uniform La₂NiO₄ distributes in ceramics, the higher the carrier migration rate is and the smaller the resistance of composite ceramic is. On the other hand, as discussed in XRD (see Fig. 1), the lattice parameters of NiO crystal in NiO-1.5LCO and NiO-1.5LNO composite ceramics are larger than that in as-sintered pure NiO ceramic, indicating that some of La-ions have substituted into NiO crystal. In the composite ceramics, partial La³⁺ ions substituted into

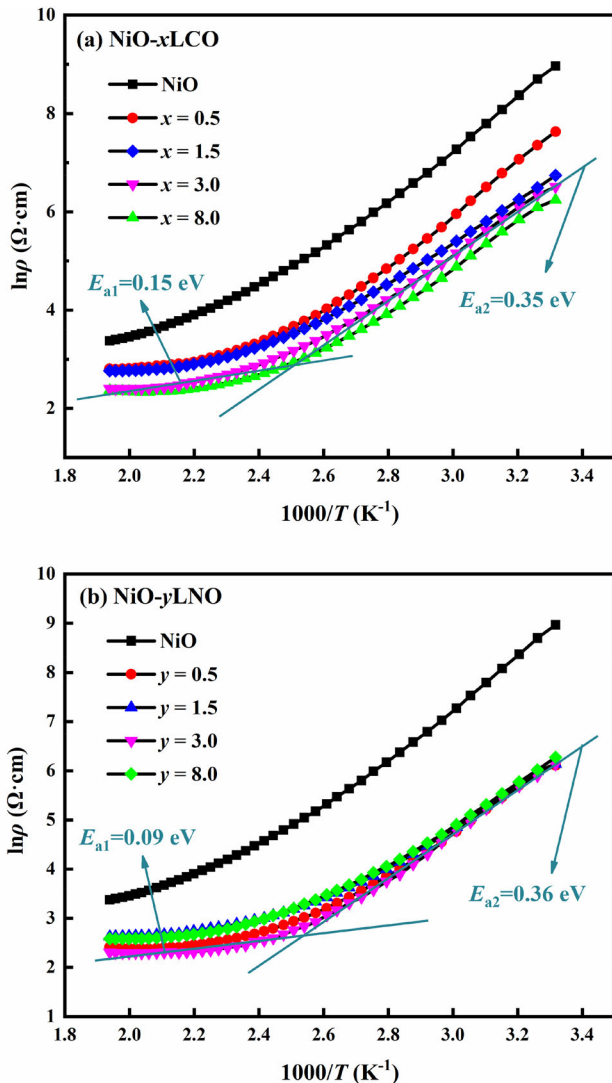


Fig. 5 Plots for temperature dependence of resistivity of prepared NiO-based ceramics, **a** NiO–*x*LCO composite ceramics, **b** NiO–*y*LNO composite ceramics

NiO lattice and acted as donors for semiconductor NiO as shown in defect reaction in Eq. (2).



As result, weakly bound electrons occurred around the point defect of La_{Ni} and can be thermally activated to conduction band in semiconductor NiO, further enhanced the ceramic conductivity.

In addition, the resistance–temperature plots of all ceramics show a typical NTC characteristic that the resistivity decreases with the temperature increases. In the testing temperature range, the relationship between $\ln\rho$ and $1000/T$ is not a single linear one and

Table 1 Comparison of room temperature resistivity ρ_{25} and material constant $B_{25/85}$ for NiO-based ceramics with various contents of La_2CuO_4 or La_2NiO_4 , the data were received from Fig. 4

Composition	ρ_{25} (Ω cm)	$B_{25/85}$ (K)
Pure NiO	7807	5563
NiO–0.5LCO	2520	5478
NiO–1.5LCO	845	4370
NiO–3.0LCO	671	4550
NiO–8.0LCO	514	4510
NiO–0.5LNO	450	4477
NiO–1.5LNO	461	4286
NiO–3.0LNO	458	4466
NiO–8.0LNO	460	4424

can be approximated as two linear regions with different slopes. According to the Arrhenius law, the $\ln\rho$ – $1000/T$ plots can be expressed as Eq. (3).

$$\rho_T = A \exp\left(\frac{\varepsilon E_{a1} + (1 - \varepsilon)E_{a2}}{kT}\right) \quad (3)$$

where, ρ_T represents resistivity at temperature T , A is a factor relating to material properties, k is the Boltzmann constant, ε ($0 \leq \varepsilon \leq 1$) is a factor relating to content of conduction mode and depends on temperature, E_{a1} and E_{a2} are activation energies of conduction for two conduction modes, respectively. For example, NiO–3.0LCO composite ceramic has activation energies of 0.15 eV at high temperature region and 0.35 eV at low temperature region. NiO–3.0LNO composite ceramic has low E_a of 0.09 eV at high temperature region and high E_a of 0.36 eV at low temperature region. The reason for the change of activation energy in different temperature ranges should be resulted from different conduction modes, e.g., band conduction of a traditional semiconductor, and other ones such as small polaron hopping mechanism. The different conduction models may play a different role in different temperature ranges, and will be discussed further in next section.

AC complex impedance spectra (CIS) of NiO–1.5LCO and NiO–1.5LNO composite ceramics were tested at different temperatures and analyzed. The results are shown in Fig. 6. Within the test temperature range, each CIS is composed of one partial arc. To reveal the grain effect and grain-boundary effect, an equivalent circuit composed of two parts elements of $(R_1\text{-CPE}_1)(R_2\text{-CPE}_2)$ is illustrated as inset in Fig. 6. Where, R_1 and R_2 represent resistances from grain

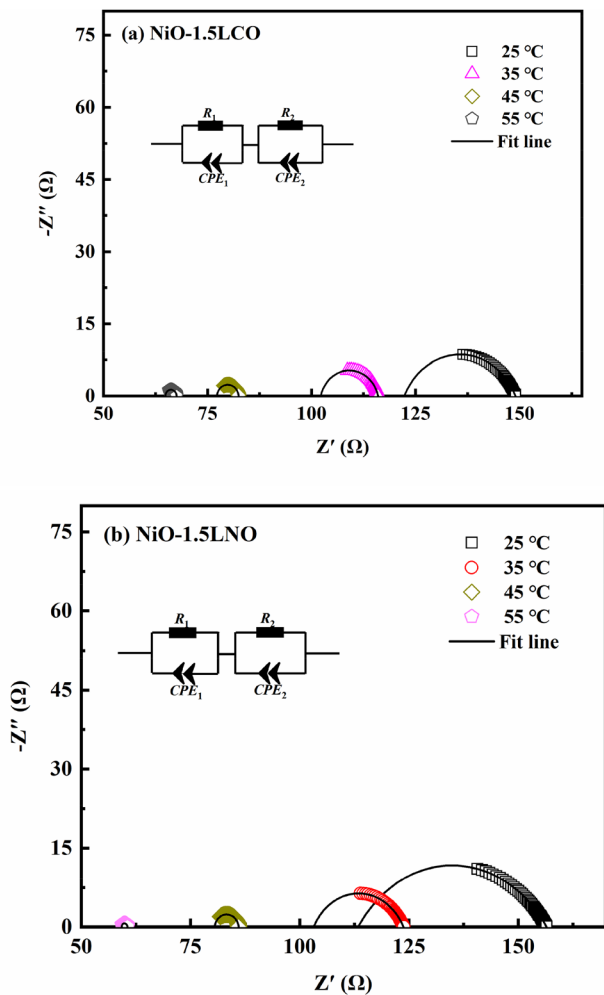


Fig. 6 Analysis of complex impedance spectra of composite ceramics at different temperatures, **a** NiO–1.5LCO, **b** NiO–1.5LNO

effect (R_g) and grain-boundary one (R_{gb}). CPE_1 and CPE_2 are the related constant phase elements. The fitted curves according to the equivalent circuit are in good agreement with the test data, indicating that each CIS is composed of two parts, i.e., grain effect and grain-boundary effect. The solid curves beyond the experimental data are calculated with a Z-view software according to the set-up equivalent circuit, in frequency region up to 10^{10} Hz.

Figure 7 shows the plots of temperature dependence of R_g and R_{gb} in NiO–1.5LCO and NiO–1.5LNO composite ceramics, obtained from fitting results in Fig. 6. Both R_g and R_{gb} exhibit NTC characteristics. At each measured temperature, R_{gb} is larger than R_g . The activation energies of conduction of grain effect (E_g) and grain-boundary effect (E_{gb})

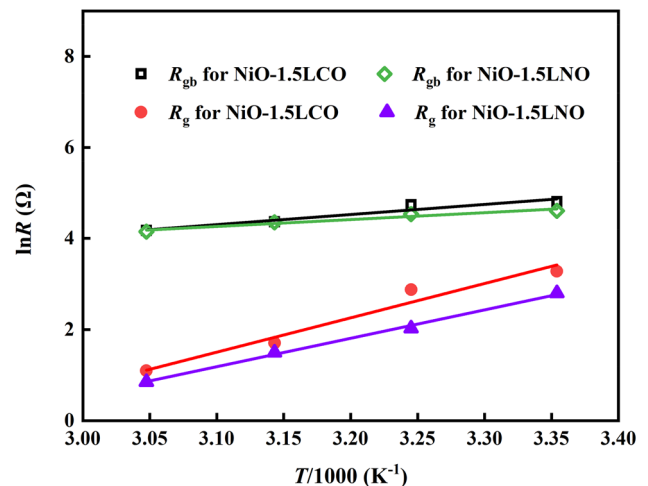
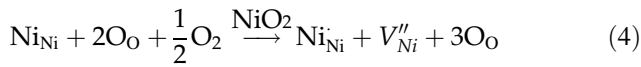


Fig. 7 Temperature dependence of resistance of grain effect (R_g) and grain-boundary effect (R_{gb}) in NiO–1.5LCO and NiO–1.5LNO composite ceramics

can be calculated according to the Arrhenius formula. E_g is 0.60 eV and E_{gb} is 0.18 eV for NiO–1.5LCO composite ceramic, E_g is 0.78 eV and E_{gb} is 0.16 eV for NiO–1.5LNO composite ceramic. These indicate that both grain effect and grain-boundary effect contributed to the NTC effect of each composite ceramic.

3.4 Discussion of conduction mode

NiO is a typical semiconductor oxide with band gap of about 3.5 eV. But an ideal perfect NiO crystal is an insulator for there is neither quasi-free electron in the conduction band level nor hole in the valence band level, i.e., there is no charge carrier in NiO. For thermal activation and/or environmental impact during material preparation process, non-stoichiometric compound occurs and lattice defects might be formed. As discussed in XRD (see in Fig. 1), the prepared NiO ceramic has rock-salt phase with lattice parameter a less than that of referred PFD No. 47-1049, indicating that vacancies and/or ions with smaller ionic radius were produced in the ceramics. Further analysis of XPS in Fig. 4 reveals that Ni^{2+} and Ni^{3+} coexist in all prepared NiO-based ceramics, indicating that the NiO phase in all ceramics should be non-stoichiometric. These indicate that Ni-vacancies formed in the NiO phase. The generation of Ni^{3+} -ions should be accompanied by formation of hole charges as described in Eq. (4).



In NiO phase, the hole charges are weakly bound at the acceptor level. The hole charges can be easily excited to the valence band level and act as the charge carriers for ceramic conduction. So the prepared pure NiO ceramic can show good conduction.

In the meanwhile, as discussed in Eq. (2), partial La³⁺ ions substituted into the NiO lattice and acted as donors for NiO phase in the composite ceramics, and further enhanced the conductivity of NiO phase in the composite ceramics. This doping effect reduced the resistance of grain effect, although the existence of La₂MO₄ (M = Ni or Cu) obviously decreased the resistance of grain-boundary effect, comparing with the results in Fig. 7 and Fig. S6. This kind of conductivity of grain effect resulted from the band conduction mode for dopant doping.

On the other hand, for the coexistence of Ni²⁺ and Ni³⁺ cations in NiO phase, in which the electronic conduction can take place for a conduction mode as-called polaron hopping that is always happened in spinel compounds and other transition metal oxides [1, 2, 12–15]. The polaron hopping conduction can be described as Ni²⁺+Ni³⁺↔Ni³⁺+Ni²⁺ in NiO-based ceramics. For the polaron hopping conduction mode, temperature-dependent conductivity (σ) is usually described by the Nernst Einstein equation shown in Eq. (5) [27].

$$\sigma = \left[\frac{Nc(1 - c)N_{\text{oct}}e^2d^2v_0}{kT} \right] \exp\left(-\frac{T_0}{T}\right) \quad (5)$$

where, *k* is the Boltzmann constant, *e* is electronic charge, *d* is hopping distance, *v*₀ is hopping frequency, *T*₀ is defined as the characteristic temperature, and *N*_{oct} is the concentration of octahedral sites. The factor *Nc*(1 - *c*) denotes the probability that Ni²⁺ and Ni³⁺ ions occupy adjacent octahedral sites, where *N* is the concentration per formula unit of sites, which are available to the charge carriers, and *c* can be defined as [Ni³⁺]/([Ni³⁺]+[Ni²⁺]). In the prepared ceramics, the content ratios of Ni²⁺ and Ni³⁺ ions ([Ni²⁺]/[Ni³⁺]) in pure NiO ceramic, NiO-1.5LCO and NiO-1.5LNO composite ceramics are 2.69:1, 2.52:1 and 2.48:1, respectively, indicating that the content of Ni³⁺ ions increased for introduction of La₂MO₄ (M = Ni or Cu). So the conductivity of NiO phase may increase accordingly with the increase

contents of La₂MO₄ (M = Ni or Cu) which is consistent with the result of Fig. 4.

At the same time, as shown in Fig. 7 and Fig. S6, the resistance from grain-boundary effect are always the main contributor for all NiO-based ceramics due to the presence of unavoidable impurities with high grain-boundary potential barrier. The charger carriers must overcome the grain-boundary potential barrier to transfer. The phases of La₂MO₄ (M = Ni or Cu) have high conductivities as shown in Fig. S4, they disperse inside the ceramics and can increase ceramic conductivity since the percolation conduction effect.

As discussed above, the conduction modes in the composite ceramics should be consisted of following factors, hopping conduction mode for the formation of non-stoichiometric compound of NiO phase, band conduction mode for La³⁺ doping in NiO phase, transition of charge carriers overcoming grain-boundary potential barrier by thermal activation (denoted as grain-boundary conduction mode), and percolation conduction for the dispersed distribution of highly conductive phases of La₂MO₄ (M = Ni or Cu). Where, electrons for hopping conduction need a certain amount of energy to get rid of the constraint of small poles and to overcome the obstacles of lattice potential barriers. So the activation energy of conduction (*E*_a) in the hopping conduction mode should always be high, accompanied by main contribution to material constants *B* value for NTC effect. In the band conduction mode, the weakly bound conductive electrons can be thermally activated easily, so this kind of conduction mode has a small contribution to *B* value of NTC effect. The grain-boundary conduction mode often contributes larger to *B* value for high potential barrier. In percolation conduction mode, the conductivity depends on the distance between high-conduction phases (La₂MO₄ (M = Ni or Cu) in present work), for the different coefficients of thermal expansion (α), the percolation conductivity changes with temperature increase. NiO has coefficient of thermal expansion (α) of about 1 × 10⁻⁵ K⁻¹, and α La₂NiO₄ is 1.39 × 10⁻⁵ K⁻¹ [28], these result in the percolation conduction became more and more significant as the temperature increases, accompanied by a decrease in related conductive activation energy and a decrease in *B* value. This might be the main reason for the results as shown in Fig. 5 that the relationship between lnρ and 1000/*T* is not a single linear one, the ceramics have lower *B* values in higher temperature region.

4 Conclusion

La_2MO_4 ($M = \text{Ni}$ or Cu) modified NiO-based ceramics are composed main phase of cubic NiO and secondary phase La_2NiO_4 or La_2CuO_4 . With modification of La_2CuO_4 or La_2NiO_4 , the sintering ability of ceramics were significantly improved, and the sintering temperature were reduced from 1380 °C of pure NiO ceramic to 1250 °C composite ceramics. All ceramics show typical NTC characteristics. For NiO- La_2CuO_4 composite ceramics, room temperature resistivity (ρ_{25}) can be adjusted in the range of 500–2500 $\Omega\cdot\text{cm}$ with change content of La_2CuO_4 , and the material constant B value can be kept in higher than 4500 K. For NiO- La_2NiO_4 composite ceramics, ρ_{25} and B value do not change much with the increase of La_2NiO_4 content, ρ_{25} are around 450 $\Omega\cdot\text{cm}$ and B values locate in range of 4286–4477 K. The electrical conductivity and NTC effect of prepared composite ceramics resulted from both grain effect and grain-boundary effect, and the conduction modes include band conduction, polaron hopping conduction, percolation conduction, and thermally activated grain-boundary transition of charge carriers.

Author contributions

ZL, HZ and LH contributed to the study conception and design. Material preparation, data collection and analysis were performed by LH, SL and ML. The first draft of the manuscript was prepared by LH, and all authors commented on previous versions of the manuscript. All authors read and approved the final manuscript.

Funding

This work is supported by the research funds from the Development Funds of Hunan Wedid Materials Technology Co., Ltd., China (Grant No. 738010241), the Foundation of the Department of Science and Technology of Guizhou province (Grant No. CG[2021]110), and the Foundation of the Department of Education of Guizhou province (Grant No. QJJ[2022]003).

Data availability

The datasets generated during and/or analyzed during the current study are available from the corresponding author on reasonable request.

Declarations

Competing interests The authors have no relevant financial or non-financial interests to disclose.

Supplementary Information: The online version contains supplementary material available at <http://doi.org/10.1007/s10854-023-10500-z>.

References

1. N. Acharya, R. Sagar, Structure and electrical properties characterization of NiMn_2O_4 NTC ceramics. *Inorg. Chem. Comm.* **132**, 108856 (2021). <https://doi.org/10.1016/j.inoche.2021.108856>
2. F. Zhang, Z. Huang, Effects of partial substitution of cations on electrical properties of Mn–Co–Ni–O thin films. *Appl. Phys. Lett.* **111**, 222103 (2017). <https://doi.org/10.1063/1.5004035>
3. Y. Liu, H. Zhang, W. Fu, Z. Yang, Z. Li, Characterization of temperature sensitivity of V-modified CuFe_2O_4 ceramics for NTC thermistors. *J. Mater. Sci. Mater. Electron.* **29**, 18797–18806 (2018). <https://doi.org/10.1007/s10854-018-0005-1>
4. J. Wang, H. Zhang, D. Xue, Z. Li, Electrical properties of hexagonal $\text{BaTi}_{0.8}\text{Co}_{0.2}\text{O}_{3-\delta}$ ceramic with NTC effect. *J. Phys. D* **42**, 235103 (2009). <https://doi.org/10.1088/0022-3727/42/23/235103>
5. Y. Zeng, Z. Li, J. Shao, X. Wang, W. Hao, H. Zhang, Electrical properties of perovskite YFeO_3 based ceramics modified by Cu/Nb ions as negative temperature coefficient thermistors. *J. Mater. Sci. Mater. Electron.* **30**, 14528–14537 (2019). <https://doi.org/10.1007/s10854-019-01824-w>
6. C. Zhou, Z. Wang, S. Wang, P. Yang, C. Chen, Preparation and characterization of negative temperature coefficient $(\text{ni,mn})_3\text{O}_4\text{--La}(\text{Mn,Ni})\text{O}_3$ composite. *J. Electroceram.* **20**, 113–117 (2008). <https://doi.org/10.1007/s10832-007-9375-0>
7. M. Chao, W. Ren, L. Wang, J.B. Xu, A.M. Chang, L. Bian, Structural, optical, and electrical properties of $(\text{Mn}_{1.56}\text{Co}_{0.96}\text{Ni}_{0.48}\text{O}_4)_{1-x}(\text{LaMnO}_3)_x$ composite thin films. *J. Eur. Ceram. Soc.* **36**, 4059–4064 (2016). <https://doi.org/10.1016/j.jeurceramsoc.2016.06.019>
8. B. Li, Z. Li, S. Zhang, D. Peng, C. Gao, H. Zhang, Electrical properties of Ga/V-modified ZnO ceramic thermistors.

- J. Mater. Sci. Mater. Electron. **32**, 28792–28806 (2021). <https://doi.org/10.1007/s10854-021-07264-9>
9. O. Pan, H. Zhang, Y. Zhang, J. Wang, Z. Li, Zr-substituted SnO₂-based NTC thermistors with wide application temperature range and high property stability. *J. Mater. Sci. Mater. Electron.* **26**, 6163–6169 (2015). <https://doi.org/10.1007/s10854-015-3197-7>
 10. S. Zhang, H. Zhang, S. Leng, Y. Wen, H. Wang, Z. Li, Electrical properties and aging characteristic of Sb/Ga co-doped single-cation oxide SnO₂. *J. Mater. Sci. Mater. Electron.* **33**, 23821–23833 (2022). <https://doi.org/10.1007/s10854-022-09140-6>
 11. X. Wang, Z. Li, W. Yan, P. Wang, H. Zhang, Electrical properties of Nb/Al-doped CuO-based ceramics for NTC thermistors. *Process. Appl. Ceram.* **14**, 47–55 (2020). <https://doi.org/10.2298/PAC2001047W>
 12. C. Gao, Z. Li, L. Yang, D. Peng, H. Zhang, Investigation of electrical and aging properties of bi-modified (Zn_{0.4}Ni_{0.6})_{1-x}Na_xO ceramic thermistors. *J. Eur. Ceram. Soc.* **41**, 4160–4166 (2021). <https://doi.org/10.1016/j.jeurceramsoc.2021.02.030>
 13. D. Peng, Z. Li, L. Huang, C. You, H. Wang, H. Zhang, Characterization of NiO based ceramics modified with Y₂O₃/BiSbO₃ for application of NTC thermistors. *J. Mater. Sci. Mater. Electron.* **33**, 11092–11105 (2022). <https://doi.org/10.1007/s10854-022-08086-z>
 14. J. Wang, H. Zhang, X. Sun, Y. Liu, Z. Li, Electrical properties and temperature sensitivity of Li/Fe-modified NiO-based ceramics as NTC thermistors. *J. Mater. Sci. Mater. Electron.* **27**, 11902–11908 (2016). <https://doi.org/10.1007/s10854-016-5335-2>
 15. Z. He, Z. Li, Q. Xiang, W. Yan, H. Zhang, Electrical properties of Y/Mg modified NiO simple oxides for negative temperature coefficient thermistors. *Int. J. Appl. Ceram. Tech.* **16**, 160–169 (2019). <https://doi.org/10.1111/ijac.13084>
 16. Y. Ichiyangi, N. Wakabayashi, J. Yamazaki, S. Yamada, Y. Kimishima, E. Komatsu, H. Tajima, Magnetic properties of NiO nanoparticles. *Phys. Rev.* **329**, 862–863 (2003). [https://doi.org/10.1016/S0921-4526\(02\)02578-4](https://doi.org/10.1016/S0921-4526(02)02578-4)
 17. W. Shin, N. Murayama, High performance p-type thermoelectric oxide based on NiO. *Mater. Lett.* **45**, 302–306 (2000). [https://doi.org/10.1016/S0167-577X\(00\)00122-1](https://doi.org/10.1016/S0167-577X(00)00122-1)
 18. H. Gallon, X. Tu, M.V. Twigg, J.C. Whitehead, Plasma-assisted methane reduction of a NiO catalyst—low temperature activation of methane and formation of carbon nanofibres. *Appl. Catal. B* **106**, 616–620 (2011). <https://doi.org/10.1016/j.apcatb.2011.06.023>
 19. Z. Ma, H. Zhang, Y. Zhang, J. Zhang, Z. Li, Electrochemical characteristics of nanostructured NiO plates hydrothermally treated on nickel foam for Li-ion storage. *Electrochim. Acta* **176**, 1427–1433 (2015). <https://doi.org/10.1016/j.electacta.2015.07.161>
 20. J.Q. Li, L. Chen, Z.X. Zhao, Y. Matsui, Short-range-oxygen order and superconducting phase separation in La₂CuO_{4+x}. *Phys. C* **341–348**, 1747–1750 (2000). [https://doi.org/10.1016/S0921-4534\(00\)00978-3](https://doi.org/10.1016/S0921-4534(00)00978-3)
 21. S. Sugai, M. Sato, T. Itoc, T. Ido, H. Takagi et al., Two-spin superexchange and four-spin cyclic exchange interactions in high T_c superconducting cuprates and isostructural La₂NiO₄. *J. Magn. Magn. Mater.* **90–91**, 631–632 (1990). [https://doi.org/10.1016/S0304-8853\(10\)80228-8](https://doi.org/10.1016/S0304-8853(10)80228-8)
 22. M. Reehuis, C. Ulrich, K. Prokes, A. Gozar, G. Blumberg, Keimer, Crystal structure and high-field magnetism of La₂CuO₄. *Phys. Rev. B* **73**, 14 (2006). <https://doi.org/10.1103/PhysRevB.73.144513>
 23. H. Spijker, D. Simon, F. Ooms, Photocatalytic water splitting by means of undoped and doped La₂CuO₄ photocathodes. *Int. J. Hydrogen Energy* **33**, 6414–6419 (2008). <https://doi.org/10.1016/j.ijhydene.2008.08.023>
 24. G. Rao, Z. Qiao, J. Liang, Thermodynamic analysis of CuO–La₂O₃ binary phase diagram. *Chin. Sci. Bull.* **8**, 577–580 (1989). (in Chinese)
 25. M. Zinkevich, F. Aldinger, Thermodynamic analysis of the ternary La–Ni–O system. *J. Alloys Compd.* **375**, 147–161 (2004). <https://doi.org/10.1002/chin.200435011>
 26. T. Lin, X. Meng, L. Shi, Catalytic hydrocarboxylation of acetylene to acrylic acid using Ni₂O₃ and cupric bromide as combined catalysts. *J. Mol. Catal. A* **396**, 77–83 (2015). <https://doi.org/10.1016/j.molcata.2014.09.027>
 27. J. Wu, Z.M. Huang, W. Zhou, C. Ouyang, Y. Hou, Y.Q. Gao, R. Chen, J.H. Chu, Investigation of cation distribution, electrical, magnetic properties and their correlation in Mn_{2-x}Co_{2x}Ni_{1-x}O₄ films. *J. Appl. Phys.* **115**, 113703 (2014). <https://doi.org/10.1063/1.4868683>
 28. D. Tripathi, T.K. Dey, Effect of particle size distribution on thermo-mechanical properties of NiO filled LDPE composites. *Bull. Mater. Sci.* **42**, 174 (2019). <https://doi.org/10.1007/s12034-019-1853-x>

Publisher's Note Springer Nature remains neutral with regard to jurisdictional claims in published maps and institutional affiliations.

Springer Nature or its licensor (e.g. a society or other partner) holds exclusive rights to this article under a publishing agreement with the author(s) or other rightsholder(s); author self-archiving of the accepted manuscript version of this article is solely governed by the terms of such publishing agreement and applicable law.